IEEE Photonics Journal
An IEEE Photonics Society Publication

Nonlinear Visible Light Communications Broadcast Channel Precoding: A New Solution for In-flight Systems

Volume 10, Number 4, August 2018

Dario Tagliaferri, *Student Member, IEEE*
Andrea Matera, *Student Member, IEEE*
Carlo Capsoni, *Senior Member, IEEE*
Umberto Spagnolini, *Senior Member, IEEE*

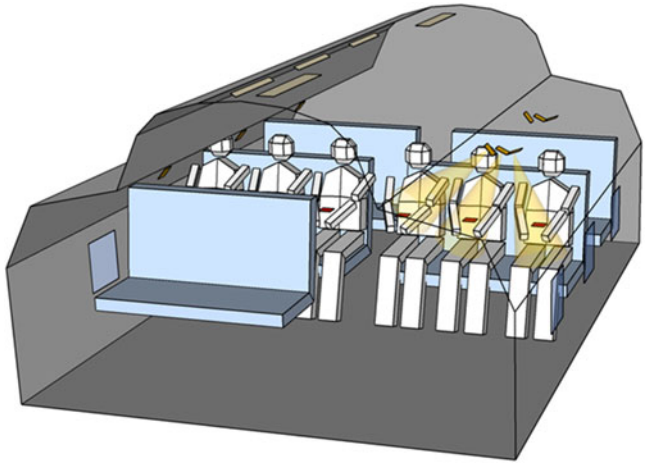

DOI: 10.1109/JPHOT.2018.2848118
1943-0655 © 2018 IEEE

IEEE photonics SOCIETY

IEEE

Nonlinear Visible Light Communications Broadcast Channel Precoding: A New Solution for In-flight Systems

Dario Tagliaferri, *Student Member, IEEE*,
Andrea Matera, *Student Member, IEEE*,
Carlo Capsoni, *Senior Member, IEEE*,
and Umberto Spagnolini, *Senior Member, IEEE*

Dipartimento di Elettronica, Informazione e Bioingegneria Politecnico di Milano, Milano 20133, Italy

DOI:10.1109/JPHOT.2018.2848118

Manuscript received May 11, 2018; revised June 7, 2018; accepted June 12, 2018. Date of publication June 22, 2018; date of current version July 4, 2018. Corresponding author: Dario Tagliaferri (e-mail: dario.tagliaferri@polimi.it).

Abstract: In this paper, we consider a multiuser multiple-input-single-output (MU-MISO) downlink visible light communication (VLC) system deployed in airplane cabins, for serving high-speed Internet to the passengers through the reading lamps. The high number of closely spaced lamps (i.e., transmitters) suggests the use of a transmit precoding scheme to suppress the strong mutual light interference and enhance the performance of the system. Constraints are the complexity of the hardware and the integration into commercial devices (smartphones, tablets, etc.). Since nominal lighting is constrained by LEDs saturation, here we adapt the Tomlinson–Harashima precoding algorithm to the on-board VLC scenario and demonstrate its definite improvement on channel capacity with respect to the unprecoded case and also to the zero-forcing precoding one. The optimum directivity of the sources trades over performance and robustness against source-receiver misalignments (i.e., the passengers' mobility) by validating MISO channels for a number of receivers' positions around the best alignment one with a ray tracer specifically designed.

Index Terms: Visible light communications, aircrafts, tomlinson-harashima precoding.

1. Introduction

Visible Light Communications (VLC) are emerging as a promising alternative to radio communications in harsh environments. Their inherent advantages are: use of unlicensed bands, E.M. pollution free and availability of low cost transmitters (LED lights) that offer a potentially high capacity per unit area system [1]. Among the various applications, on-aircraft VLC systems are gaining large attention in recent years, as a possible technique to provide low cost, ubiquitous and green access to high speed Internet through the usage of the LED reading lamps, for which the communication function would be superposed to their natural illumination one. VLC offers an inexpensive and scalable alternative to the existing low-bandwidth Wi-Fi-based infrastructure [2], that adapts to the asymmetric traffic conditions of the entertaining and multimedia services. VLC-based solution mimics femto-cell systems by exploiting the available LED reading lamps to serve the passengers' terminals (which can be added into or externally to laptops, tablets, smartphones etc.) with a point-to-point wireless downlink Intensity-Modulated/Direct-Detected (IM/DD) visible light communication.

The reading lamps can be connected to the external communications system by any technology (e.g., power line communication [3] or optical fiber [4]). Each user device logs on to "its own" cell through a proper uplink transmission protocol (typically infrared, IR). High QoS is dependent on adequate values of Signal-to-Interference-plus-Noise Ratio (SINR). The large number of closely spaced non-directive transmitters makes the communication challenging, due to the interferences that are generated while many sources of light inside the cabin (e.g., ceiling, sidewall, dome lights, solar radiation entering through the fuselage windows) contribute to increase the noise at the receivers' front-end. The possibility of in-flight VLC was already introduced and investigated in [5] [6], while the specific problem of exploring the interference and the Signal-to-Interference Ratio (SIR) was reported in [7], for a simple airplane cabin geometry and sources-receivers configuration. A complete characterization of the SINR inside a realistic airplane cabin has been presented in [8] under the hypothesis of perfect alignment between transmitters and receivers, showing promising results in case of highly directive lamps. However, as soon as the device is moved (e.g., user moves the device from hand to hand), the use of a LED with a wider beamwidth could be a viable solution to guarantee seamless connectivity while reducing the Mutual Light Interference (MLI) to acceptable values with a proper technique. Apart from the most common frequency or time division multiplexing schemes (FDM/TDM, respectively) that cannot be accommodated within the limited electrical bandwidth of common LED lamps [9], MLI reduction could be by Colour Division Multiplexing (CDM) [10], [11], by assigning a different colour to each data-stream. Despite the spectral efficiency of CDM approach (each source transmits on the same electrical bandwidth), it has the inherent disadvantage of having to equip the receiving terminals with more additional optical components and analog decoding chains to receive separately every possible colour, thus increasing the costs and the complexity of the realization.

In this paper, we explore the possibility of using a multi-stream Transmitter Precoding (TP) approach to mitigate MLI at the receivers, by exploiting the knowledge of the channel characteristics from each transmitter to each receiver. When multiple sources are coordinated (acting as a single, whole transmitter) to transmit information to multiple devices equipped with one single receiver, the system is called Multi-User-Multiple-Input Single-Output (MU-MISO), and the one-to-many communication channel is identified as "broadcast". In particular, Tomlinson-Harashima Precoding (THP) is a well-suited solution for MU-MISO communication systems [12], [13]. Even if the literature on MU-MISO systems is well detailed, the VLC scenario contains some peculiarities:

- VLC is a special type of Intensity-Modulation/Direct-Detection Optical Wireless Communication (IM/DD OWC), so the transmitter uses real-valued and non-negative signals instead of complex and bipolar ones;
- each LED transmitting unit has two power constraints: the average value of the emitted signal (average optical intensity intended for illumination) and the maximum peak amplitude (maximum optical intensity) limited by the LED technology or by its input linearity range.

1.1 Related Works

The concept of MU-MISO VLC systems is close to that of multiple-input multiple-output (MIMO) optical wireless communication, which dates back to [14]. More recently, Hsu *et al.* [15] proposed and demonstrated a 3×3 single-user MIMO VLC system using commercial available phosphorescent white LEDs and performing Zero-Forcing (ZF) channel equalization at the single receiver. However, the MU-MISO VLC system considered here is for multiple devices that are geographically distributed so that no joint receiver processing can be performed. Instead, signal processing should be entirely shifted at the transmitter side and applied prior to signal transmission in form of precoding. Transmitter precoding techniques for MU-MISO VLC systems are in [16]–[19]. These papers proposed linear or non-linear techniques for ideal VLC scenarios within an empty room, thus not accounting for complex reverberating environments. In Li *et al.* [16], Zero-Forcing (ZF) and Minimum Mean Squared Error (MMSE) linear precoding techniques were analyzed in terms of average Bit Error Rate (BER) and Mean Square Error (MSE) performance through simulations in an empty room, where an arbitrary number of receivers were randomly placed. In Ma *et al.* [17] the

application scenario is again an empty room, and authors proposed two linear precoding schemes, obtained through sum-MSE minimization and minimal illumination level. A different approach has been followed by Pham *et al.* [19], who proposed a MU-MISO VLC system optimization in terms of lower and upper bounds of VLC channel capacity (i.e., mutual information between input and output) and linear ZF precoding techniques. Non-linear precoding for VLC has been first considered in Yu *et al.* [18], that compared a linear ZF precoding scheme with a non-linear one based on Zero-Forcing-Dirty Paper Coding (ZF-DPC) with a remarkable spectral efficiency gain. ZF-DPC represents a theoretical upper bound that can be attained by pre-canceling methods such as the proposed THP, that is compared herein to ZF-DPC.

1.2 Contributions

In this work we adapted the Tomlinson-Harashima Precoding (THP) to a VLC system and evaluated the performance for a realistic highly-reverberating scenario inside an airplane passenger cabin. The choice is mainly motivated by the fact that the non-linear transmitter precoding allows to mitigate multi-user interference still bounding the transmitted power. THP is very promising for VLC applications, since the amplitude constraint to be imposed on the emitted signal can be inherently fulfilled. Moreover, inside an airplane cabin the users' mobility is very limited and the optical channel is quasi-static, or slowly time varying. This condition is suited for the application of a complex algorithm such as THP, which needs an higher computation overhead with respect to ZFP, because the precoding matrix is recalculated much less frequently.

In particular, the contributions of the paper are three-fold:

1) we first developed a realistic model of a passenger cabin with a certain number of reading lamps and receivers to compute the VL channel matrixes with [8];
2) we adapted THP to VLC and demonstrated the performance gain with respect to ZFP, comparing THP with the ZF-DPC upper bound as indicated in [18], for varying emission angles and degree of coordination by the size of the precoding matrix;
3) we identified an optimal configuration of the precoding system that guarantees the best compromise among channel capacity maximization, precoding complexity, robustness against source-receiver misalignments, and lamps directivity (in order not to dazzle the adjacent passengers and avoid discomfort situations).

1.3 Notation

Bold upper- and lower-case letters describe matrices and column vectors. $[\mathbf{A}]_{ij} = a_{ij}$ denotes the ij-th element of matrix $\mathbf{A}$. Letters $\mathbb{R}$, $\mathbb{R}_{\geq 0}$ and $\mathbb{C}$ refer to real, non-negative real and complex numbers, respectively. We denote matrix inversion, transposition and conjugate transposition as $(\cdot)^{-1}$, $(\cdot)^{T}$, $(\cdot)^{H}$. Matrix $\mathbf{I}$ is an identity matrix of appropriate size, $\mathrm{E}[\cdot]$ is the statistical expectation, $\mathrm{diag}(\mathbf{A})$ is a diagonal matrix containing the main diagonal elements of matrix $\mathbf{A}$. Finally, $\|\mathbf{x}\|_1 = \sum_i |x_i|$ and $\|\mathbf{x}\|_2 = \sqrt{\sum_i |x_i|^2}$ are the l_1- and l_2- norms of vector $\mathbf{x}$, respectively.

1.4 Organization

The paper is organized as follows: Section 2 reports a description of the ray tracing that we used to simulate the visible light channel inside the cabin and retrieve the channel matrixes and mutual interference; Section 3 illustrates the system model and sets the VLC analytical constraints for precoding; Section 4 reviews ZFP and details THP adapted to VLC scenarios; Section 5 presents the results of the simulations we performed to demonstrate the validity of our proposal, while Section 6 draws some conclusions.

2. Channel Generation by Ray Tracing

In order to test the performance of the proposed algorithms, we have generated the optical channel matrixes and computed the SINR by using the Modified MonteCarlo (MMC) ray tracer tool detailed in [8], originally developed for the characterization of visible and infrared (IR) light propagation inside any arbitrary-shaped space. The tool in [8] provides the Channel Impulse Response (CIR) from each modulated light source to each receiver in the space, together with the background light level (which is the amount of optical power due to all the non-modulated sources of radiation) and the SINR at the receiving side. The CIRs are computed for a set of testing wavelengths chosen either in visible or in near-IR range and considering an arbitrary number of reflections. The final result is a function of the specific source-receiver pair (j, k), the wavelength λ and the time t: CIR is hereafter indicated with $h[t, j, k, \lambda]$. The background light levels composed by the optical power from the illumination fixtures and from the solar radiation entering through the windows (the latter being modeled according to [20] and [21]). The SINR at the k-th photodiode receiver is

$$\mathrm{SINR}_k = \frac{i_{s,k}^2}{i_{int,k}^2 + \sigma_{n,k}^2}, \tag{1}$$

where the numerator is the squared electrical current generated by the useful modulated light sources and the denominator is the sum of the squared electrical current generated by the interfering light signals (which are in the same electrical band of the useful ones) plus the overall electrical noise power $\sigma_{n,k}^2$. As motivated in the introduction, in this work we consider standard phosphor-based LED as VLC sources, thus we choose as testing wavelengths for every simulation the red, green and blue peaks (i.e. 460 nm, 532 nm and 650 nm) as in [22]. Hereafter, we consider the channel as frequency-flat within the bandwidth of interest that is set to $B = 20$ MHz. The electrical current for the signal of interest is expressed as

$$i_{s,k} = \sum_{t=0}^{N_t} \sum_{j \in \mathcal{K}_{\mathcal{U}}} \sum_{\lambda \in \mathcal{W}} \underbrace{P_T[j, \lambda] \cdot h[t, j, k, \lambda] \cdot \eta[k, \lambda]}_{i_R[t,j,k,\lambda]}, \tag{2}$$

where $P_T[j, \lambda]\,[W]$ is the optical power transmitted by the j-th source at wavelength λ and $\eta[k, \lambda]$ is the k-th photodetector spectral responsivity measured in $[A/W]$. The product of the three terms is the generated photocurrent at the receiver $i_R[t, j, k, \lambda]$. The total electrical current at the receiver is the obtained by summing over the time grid on which the CIR is computed (thanks to the frequency-flat hypothesis), the set of wavelengths $\mathcal{W}$ and the set of useful sources ($\mathcal{K}_{\mathcal{U}}$). The interfering current $i_{int,k}$ has the same expression of Eq. (2), with the only difference that the summation spans the set of interfering sources, while the electrical noise power $\sigma_{n,k}^2$ is computed as:

$$\sigma_{n,k}^2 = 2\,e\,B\,\left\{i_{bg,k} + i_{s,k} + i_{int,k} + i_{dark,k}\right\} + \sigma_{th,k}^2, \tag{3}$$

where the first term is the overall shot noise caused by the sum of the electrical currents generated respectively by the background light ($i_{bg,k}$), the signal and interfering lights ($i_{s,k} + i_{int,k}$) and the dark current of the photodector ($i_{dark,k}$) [23] while the second one is the thermal noise variance (the input referred noise density $i_{\mathrm{rms}}\,\left[A/\sqrt{Hz}\right]$ of the front-end's first amplifying stage).

The channel matrix is then computed as an intensity-one:

$$\mathbf{H} = \left\{h_{j,k}\right\}, \qquad h_{j,k} = \sum_{t=0}^{N_t} \sum_{\lambda \in \mathcal{W}} h[t, j, k, \lambda], \tag{4}$$

where $h_{j,k}$ is the channel coefficient between the k-th transmitter and the j-th receiver, and results from the summation over the time grid on which the complete CIR $h\,[t, j, k, \lambda]$ is computed and over the set of wavelengths $\mathcal{W}$ for white-light VLC.

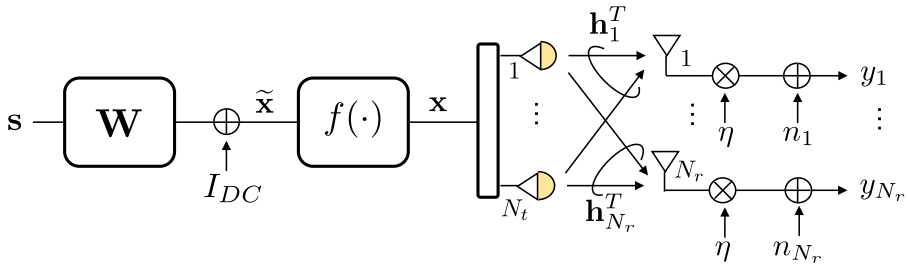

Fig. 1. Downlink VLC system model with transmitter precoding. The N_t signals (vector **s**) are precoded by matrix **W** and then transmitted onto the VLC channel by means of N_t non-directive sources (LEDs) to N_r single-PD users.

3. System Model

In this work we consider the downlink of a general MU-MISO VLC system consisting in N_t LED transmitters serving N_r single-photodiode users (i.e., aircraft passengers), as shown in Fig 1.

3.1 VLC Downlink Channel

The downlink channel from the LEDs to the users is a frequency-flat VLC channel, such that the signal received at the k-th user is

$$y_k = \eta \mathbf{h}_k^T \mathbf{x} + n_k, \tag{5}$$

where η is the photodiode (PD) responsivity, $\mathbf{h}_k^T \in \mathbb{R}_{\geq 0}^{1\times N_t} = \left[h_{1,k}, h_{2,k}, \ldots, h_{N_t,k}\right]$ is the non-negative, real-valued vector denoting the channel coefficients from all the LEDs to the k-th single-photodetector user, $\mathbf{x} \in \mathbb{R}_{\geq 0}^{N_t\times 1}$ represents the emitted optical power signal and $n_k \sim \mathcal{N}(0, \sigma_{n,k}^2)$ is the overall noise fluctuation current at the k-th receiver which can be reasonably modeled as zero-mean additive Gaussian process [24] with variance $\sigma_{n,k}^2$ (computed with (3)). Gathering all the received user signals, we obtain the canonical MU-MISO model as

$$\mathbf{y} = \eta \mathbf{H}\mathbf{x} + \mathbf{n}, \tag{6}$$

where $\mathbf{y} = [y_1, y_2, \ldots, y_{N_r}]^T$ is the signal received by all the users, $\mathbf{H} = [\mathbf{h}_1, \mathbf{h}_2, \ldots, \mathbf{h}_{N_r}]^T \in \mathbb{R}_{\geq 0}^{N_r\times N_t}$ is the compound channel matrix defined as in (4) and $\mathbf{n} \sim \mathcal{N}(\mathbf{0}, \mathbf{R}_n)$ is the overall zero-mean additive uncorrelated colored Gaussian noise with covariance $\mathbf{R}_n = \text{diag}(\sigma_{n,1}^2, \sigma_{n,2}^2, \ldots, \sigma_{n,N_r}^2)$.

3.2 Transmitter Constraints

The transmitted signals **x** are obtained as

$$\mathbf{x} = f\left(\tilde{\mathbf{x}}\right), \tag{7}$$

where $\tilde{\mathbf{x}}$ are the electrical drive current signals at the LEDs input and $f(\tilde{\mathbf{x}})$ is the LED optical power (or, equivalently, luminous intensity) vs drive current characteristic, assumed hereafter to be the same for each LED. As typical for white phosphorescent LEDs [25], for a drive input current $\tilde{x}_k$ in the range $[0, I_{\max}]$ it is approximately linear as

$$f(\tilde{x}) \approx \gamma \cdot \tilde{x}, \tag{8}$$

where γ is the so-called LED conversion factor that maps $[0, I_{\max}]$ into optical power $[0, P_{\max}]$ [17].

Since we use a transmitter precoding technique, the drive current signals at the LEDs input are obtained as

$$\tilde{\mathbf{x}} = \mathbf{W}\mathbf{s} + \mathbf{i}_{DC}, \tag{9}$$

where $\mathbf{s} = [s_1, s_2, .., s_{N_r}]^T \in \mathbb{R}^{N_r \times 1}$ are the zero-mean, uncorrelated symbols to be transmitted to the N_r users, whose amplitudes are limited as

$$|s_k| \in [-d_k, +d_k], \tag{10}$$

$\mathbf{W} \in \mathbb{R}^{N_t \times N_r}$ is the precoding matrix, and $\mathbf{i}_{DC} \in \mathbb{R}_{\geq 0}^{N_t \times 1}$ is the vector of DC offset currents added to the signal in order to ensure the non-negativity of the output. Vector $\mathbf{s}$ can include either pulse-amplitude modulated (PAM) symbols or quadrature-amplitude modulated (QAM) ones (see *Remark 1*). In the following, we assume without loss of generality that the DC currents I_{DC}^k are the same for all the LEDs, so $\mathbf{i}_{DC} = I_{DC}\mathbf{1}$ where $\mathbf{1}$ is a column vector of all ones. Therefore, the average transmitted optical power at each LED is

$$\mathrm{E}[x_k] = \gamma \mathrm{E}[\tilde{x}_k] = \gamma \mathrm{E}[\mathbf{w}_k^T \mathbf{s} + I_{DC}] = \gamma I_{DC} = P_T. \tag{11}$$

From (9), the amplitude constraints on the transmitted signals can be written as:

$$0 \leq \mathbf{w}_k^T \mathbf{s} + I_{DC} \leq I_{\max}, \tag{12}$$

where, $\mathbf{w}_k^T$ is the k-th row of the precoding matrix $\mathbf{W}$. Without loss of generality, we choose the DC current I_{DC} to be exactly half of the LED dynamics ($I_{DC} = I_{\max}/2$), and the maximum amplitude of the electrical PAM modulated symbol to be $d_k = I_{DC}$, so as to exploit the full dynamic range of the transmitter. From (10) and considering all the previous assumptions, it follows that

$$0 \leq \mathbf{w}_k^T \mathbf{s} \leq I_{DC} \quad \rightarrow \quad \left\|\mathbf{w}_k^T\right\|_1 d_k \leq I_{DC}, \quad \rightarrow \quad \left\|\mathbf{w}_k^T\right\|_1 \leq 1 \qquad \forall k = 1, .., N_t. \tag{13}$$

It is easy to show that under these assumptions the constraint in (12) is always satisfied.

To tackle the VLC downlink amplitude constraint at the transmitting LEDs, it is convenient to scale the precoding operator $\mathbf{W}$ as

$$\mathbf{W} = \tilde{\mathbf{W}} \frac{1}{\beta}, \tag{14}$$

where $\tilde{\mathbf{W}}$ is the MU-MISO precoder and β enforces the power constraint $I_{\max}$ (12), which can be rewritten as

$$\left\|\mathbf{w}_k^T\right\|_1 = \frac{1}{\beta}\left\|\tilde{\mathbf{w}}_k^T\right\|_1 \leq 1, \quad \forall k = 1, .., N_t, \tag{15}$$

where $\tilde{\mathbf{w}}_k^T$ is the row of the matrix $\tilde{\mathbf{W}}$ which precodes the signal to be transmitted by the k-th LED. From (15) the VLC amplitude constraint is always fulfilled for

$$\beta = \left\|\tilde{\mathbf{W}}^T\right\|_\infty = \max_k \left\|\tilde{\mathbf{w}}_k^T\right\|_1, \tag{16}$$

with the $(\infty)-$norm $\|\mathbf{A}\|_\infty$ denoting the maximum absolute column sum of the matrix $\mathbf{A}$ (i.e., the maximum column l_1-norm of matrix $\mathbf{A}$).

Remark 1: The analytical treatment of the precoding problem adopted here applies both to conventional single-carrier and to multi-carrier transmissions, such as the MU-MISO OFDM system discussed in [26]. In this last case, Eq. (9) describes the precoding operation applied to each OFDM subcarrier.

3.3 Signal-to-Interference-Plus-Noise Ratio With Precoding

At this point, it is useful to rewrite the expression of the k-th user's SINR highlighting the precoding scheme defined by $\mathbf{W}$ in terms of the elements of the equivalent channel matrix

$$\tilde{\mathbf{H}} = \mathbf{HW}. \tag{17}$$

To get it, we note that if the constraints in (13) are satisfied, the overall signal (6) received at the users becomes

$$\mathbf{y} = \eta\gamma \mathbf{HWs} + \eta\gamma I_{DC}\mathbf{H1} + \mathbf{n}, \tag{18}$$

where the DC current is removed by a filter at the receiver leading to the equivalent MU-MISO model

$$\mathbf{y} = \eta\gamma\widetilde{\mathbf{H}}\mathbf{s} + \mathbf{n}. \tag{19}$$

It follows that the electrical signal received at the k-th single-PD user yields

$$y_k = \eta\gamma\widetilde{h}_{kk}s_k + \eta\gamma\sum_{j\neq k}\widetilde{h}_{kj}s_j + n_k, \tag{20}$$

where the first term is the information of interest, the second term represents the residual interference light from all the other transmitters and the last one is the noise. The achievable SINR is therefore:

$$\widetilde{\mathrm{SINR}}_k = \frac{i_{s,k}^2}{i_{int,k}^2 + \sigma_{n,k}^2} = \frac{\gamma^2\eta^2 I_{DC}^2\widetilde{h}_{kk}^2}{\gamma^2\eta^2 I_{DC}^2\sum_{j\neq k}\widetilde{h}_{kj}^2 + \sigma_{n,k}^2} = \frac{\eta^2\widetilde{h}_{kk}^2 P_T^2}{\eta^2 P_T^2\sum_{j\neq k}\widetilde{h}_{kj}^2 + \sigma_{n,k}^2}. \tag{21}$$

Hence, the transmission rate for user k-th and the sum rate can be computed respectively as

$$r_k = \frac{1}{2}\log_2\left(1 + \widetilde{\mathrm{SINR}}_k\right), \qquad R = \sum_{k=1}^{N_r} r_k, \tag{22}$$

assuming the overall disturbance at the denominator in (21) is modeled as a zero-mean Gaussian process with variance $\eta^2 P_T^2\sum_{j\neq k}\widetilde{h}_{kj}^2 + \sigma_{n,k}^2$.

4. VLC Downlink Precoding

In this section, the VLC precoding scheme is detailed with the aim to take benefit from interference, which is conventionally perceived as an impairment for the communication. In particular, in this work we focus on Zero-Forcing (ZF) precoding which forces to zero all the interference between the N_r users. Hence, the precoding matrix $\mathbf{W}$ is designed to fully cancel the MLI in the VLC channel, which is mathematically described by the diagonalization of the VLC channel matrix $\mathbf{H}$ as [27]

$$\widetilde{\mathbf{H}} = \mathbf{HW} = \mathrm{diag}(\widetilde{h}_{11}, \widetilde{h}_{22}, \ldots, \widetilde{h}_{N_rN_r}), \tag{23}$$

where $\widetilde{h}_{kk}$ denotes the equivalent channel gain for the k-th user.

It follows that in the case of ZF precoding the decision variable at the k-th single-PD user in (20) yields

$$y_k = \eta\gamma\widetilde{h}_{kk}s_k + n_k, \tag{24}$$

and the corresponding SINR simplifies to

$$\widetilde{\mathrm{SINR}}_k = \frac{\eta^2\widetilde{h}_{kk}^2 P_T^2}{\sigma_{n,k}^2}. \tag{25}$$

Finally the transmission rate r_k with precoding is computed as

$$r_k = \frac{1}{2}\log_2\left(1 + \frac{\eta^2\widetilde{h}_{kk}^2 P_T^2}{\sigma_{n,k}^2}\right). \tag{26}$$

By the comparison between (21) and (25), it can be noticed that the interference term in the SINR expression in (21) is completely cancelled due to the effect of precoding.

In the following, linear and non-linear zero forcing precoding approaches are reviewed and adapted to the peculiarities of the VLC scenario.

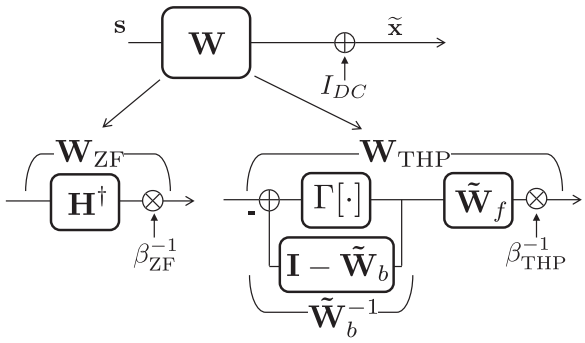

Fig. 2. VLC precoding schemes: linear Zero-Forcing (ZF) vs Tomlinson-Harashima Precoding (THP)

4.1 Linear Zero Forcing Precoding

In linear ZF the VLC channel $\mathbf{H}$ is inverted by the linear transformation $\tilde{\mathbf{W}}_{\mathrm{ZF}}$ as

$$\tilde{\mathbf{W}}_{\mathrm{ZF}} = \mathbf{H}^{\dagger}, \tag{27}$$

where $\mathbf{A}^{\dagger} = \mathbf{A}^{H}\left(\mathbf{A}\mathbf{A}^{H}\right)^{-1}$ denotes the right Moore–Penrose pseudo-inverse of matrix $\mathbf{A}$. It is easy to prove that the ZF condition (23) is satisfied, i.e.,

$$\mathbf{H}\mathbf{W}_{\mathrm{ZF}} = \frac{1}{\beta_{\mathrm{ZF}}}\mathbf{I}, \tag{28}$$

and that the rate for user k-th is

$$r_k \leq \frac{1}{2}\log_2\left(1 + \frac{1}{\beta_{\mathrm{ZF}}^2}\cdot\frac{r_f^2 P_T^2}{\sigma_{n,k}^2}\right), \tag{29}$$

where β_{ZF} is computed by (16).

4.2 Tomlinson-Harashima Precoding

Linear ZF precoding is known to lead to an extremely high scaling factor $\beta_{\mathrm{ZF}} \gg 1$ to contrast the amplitude peaks of the encoded symbols which severely degrades the transmission rates for all the users (29).

Tomlinson-Harashima Precoding (THP) for the VLC downlink is a non-linear successive interference cancellation precoding scheme, conventionally based on ZF criteria, that inherently accounts for amplitude dynamics. The main idea behind THP is to implement the VLC channel inversion by successively canceling previously encoded symbols, still limiting their amplitude by a non-linear modulo operation on amplitudes. The THP scheme is depicted in Fig. 2, where the precoding matrix $\tilde{\mathbf{W}}_{\mathrm{THP}}$ is decomposed in two sub-matrices as

$$\tilde{\mathbf{W}}_{\mathrm{THP}} = \tilde{\mathbf{W}}_f\tilde{\mathbf{W}}_b^{-1}, \tag{30}$$

where $\tilde{\mathbf{W}}_f \in \mathbb{R}^{N_t\times N_r}$ is a linear matrix with orthonormal columns (i.e., feed-forward filter) and $\tilde{\mathbf{W}}_b \in \mathbb{R}^{N_r\times N_r}$ (feedback filter) is a lower-triangular matrix with unit values along the main diagonal. As anticipated before, the key characteristic which makes THP an attractive solution for applications with strict transmit power (or amplitude in this case) constraints (e.g., DSL communication systems [28], [29]) is that the inversion of the triangular matrix $\tilde{\mathbf{W}}_b$ is performed by backward substitution together with a non-linear modulo operator $\Gamma[\cdot]$ (see feedback block in Fig. 2) which limits the amplitude of the encoded symbols within the boundaries of the original signal constellation.

Feed-forward filter $\tilde{\mathbf{W}}_f$ and feedback filter $\tilde{\mathbf{W}}_b$ are typically obtained [28] by the QR decomposition of the VLC channel matrix $\mathbf{H}$ as

$$\mathbf{H}^T = \mathbf{QR} = [\mathbf{Q}_1, \mathbf{Q}_2]\begin{bmatrix}\mathbf{R}_1 \\ \mathbf{0}\end{bmatrix}, \tag{31}$$

then

$$\tilde{\mathbf{W}}_f = \mathbf{Q}_1, \quad \tilde{\mathbf{W}}_b = \mathrm{diag}(\mathbf{R}_1)^{-1}\mathbf{R}_1^T, \tag{32}$$

where $\mathbf{Q}_1 \in \mathbb{R}^{N_t \times N_r}$ contains the first N_r orthonormal columns of the unitary matrix $\mathbf{Q} \in \mathbb{R}^{N_t \times N_t}$, $\mathbf{R}_1 \in \mathbb{R}^{N_r \times N_r}$ is an upper triangular matrix and $\mathrm{diag}(\mathbf{R}_1) \in \mathbb{R}^{N_r \times N_r}$ is a diagonal matrix that contains the main diagonal entries of $\mathbf{R}_1$. It can be shown that the ZF condition (23) is satisfied:

$$\begin{aligned}\mathbf{HW}_{\mathrm{THP}} &= \mathbf{HW}_f\tilde{\mathbf{W}}_b^{-1}/\beta_{\mathrm{THP}} \\ &= \mathbf{R}_1^T\mathbf{Q}^T\mathbf{QR}_1^{-T}\mathrm{diag}(\mathbf{R}_1)/\beta_{\mathrm{THP}} \\ &= \mathrm{diag}(\mathbf{R}_1)/\beta_{\mathrm{THP}}.\end{aligned} \tag{33}$$

Similarly to (22), (26), the rate of user k-th is therefore

$$r_k \leq \log_2\left(1 + \frac{|r_{kk}|^2}{\beta_{\mathrm{THP}}^2} \cdot \frac{\eta^2 P_T^2}{\sigma_{n,k}^2}\right), \tag{34}$$

where r_{kk} is the k-th diagonal entry of matrix $\mathrm{diag}(\mathbf{R}_1)$ and β_{THP}^2 is computed as in (16).

To prove the benefits of THP with respect to linear ZFP for the considered VLC architecture, let us focus on the interpretation of the scaling factor β, whose value is proportional to the amplitude penalty to be paid by performing a complete channel inversion at the transmitter side. Let us consider the Tomlinson-Harashima precoded symbols $\tilde{\mathbf{x}} = \tilde{\mathbf{W}}_b^{-1}\mathbf{s}$ at the output of the feedback block. Notice that in case of M-ary square QAM input symbols $\mathbf{s}$, the encoded symbols $\tilde{\mathbf{x}}$ are approximately uncorrelated with only a slight power increment with respect to the input symbols [12] (i.e., $\sigma_{\tilde{x}}^2 = \frac{M}{M-1}\sigma_s^2$) that is bounded to maximum 1.25 dB [29], hence neglected in simulation results (Sect. 5). As a consequence of the modulo operation in THP and of the aforementioned assumption, the maximum amplitude of the symbols at the output of the feedback filter is approx. the same as the maximum signal amplitude at the input, i.e.,

$$\max_k |\tilde{x}_k| \approx \max_k |s_k|. \tag{35}$$

Let us now consider the k-th precoded symbol

$$x_k = \frac{1}{\beta_{\mathrm{THP}}}\left[\tilde{\mathbf{W}}_f\tilde{\mathbf{x}}\right]_k = \frac{1}{\beta_{\mathrm{THP}}}\left[\mathbf{Q}_1\tilde{\mathbf{x}}\right]_k = \frac{1}{\beta_{\mathrm{THP}}}\mathbf{q}_{1,k}^T\tilde{\mathbf{x}}, \tag{36}$$

with $[\mathbf{a}]_k$ denoting the k-th element of vector $\mathbf{a}$ and $\mathbf{q}_{1,k}^T \in \mathbb{R}^{1\times N_r}$ the k-th row of matrix $\mathbf{Q}_1$. It directly follows from (13) and (36) that the amplitude of the k-th transmit symbol x_k is constrained by

$$|x_k| = \frac{1}{\beta_{\mathrm{THP}}}\left\|\mathbf{q}_{1,k}^T\right\|_1 \leq 1. \tag{37}$$

Therefore, the VLC amplitude constraint is always satisfied if

$$\beta_{\mathrm{THP}} = \max_k \left\|\mathbf{q}_{1,k}^T\right\|_1. \tag{38}$$

The key observation is that $\mathbf{q}_{1,k}^T \in \mathbb{R}^{1\times N_r}$ contains only the first N_r entries of the k-th unit-length row $\mathbf{q}_k^T$ of the original unitary matrix $\mathbf{Q}$ coming from (31), hence,

$$\beta_{\mathrm{THP}} = \max_k \left\|\mathbf{q}_{1,k}^T\right\|_1 \overset{(a)}{\leq} \max_k \left\|\mathbf{q}_k^T\right\|_1 \overset{(b)}{\leq} \sqrt{N_t}\left\|\mathbf{q}_k^T\right\|_2 = \sqrt{N_t}, \tag{39}$$

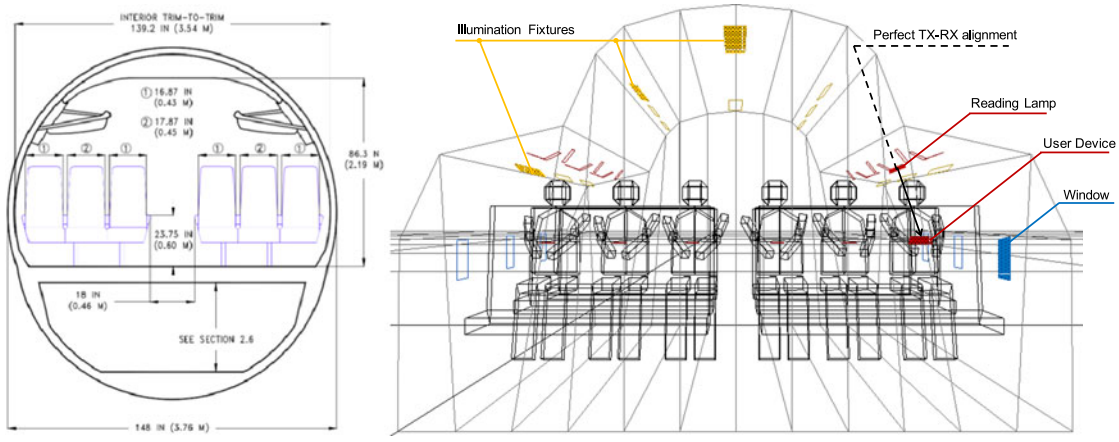

(a) (b)

Fig. 3. Boing 737 fuselage. (a) Section. (b) Frontal view (Autodesk 3DS Max).

where the equality in $^{(a)}$ holds if $N_t = N_r$ (i.e., the VLC channel to be precoded is squared) and $^{(b)}$ comes from the inequality between l_2- and l_1-norm. Therefore, if THP is employed for VLC, the power penalty to be paid is bounded by the square root of the number of transmitting LEDs N_t, which is in general much lower than β_{ZF}.

5. Simulation Settings and Numerical Results

5.1 Airplane Cabin Generation and Simulation Settings

By using Autodesk 3DS Max, we generated a section of the internal part of a Boeing 737 fuselage as in Fig. 3(a) [30], that considers 3 seat tiers, each one including 6 adjacent seats divided by the central corridor in two 3-seats groups. Each seat is equipped with its own reading lamp perfectly pointed on the users (receivers) so that overall there are $N_{t,tot} = 18$ transmitting LEDs in the system. For performance evaluation, we considered only the $N_r = 6$ passenger's models sitting in the central tier, each one with a receiving terminal. As proved in [8], with the purpose of simulating the visible light propagation in the space and successively compute the channel matrixes $\{\mathbf{H}\}$ and the electrical noise powers $\{\sigma^2_{n,k}\}$ (see Sect. II), it is sufficient to model 3 seat tiers only. This is due to the fact that the effect of further emitting devices has not significant impact on the considered N_r central-tier passengers. In particular, in this work we assumed user devices equipped with a single Osram BPW 34 Si-PIN photodetector (PD) characterized by a 7.02 mm^2 area, 60° field-of-view (FOV), 23 MHz bandwidth (with 10 V reverse voltage), 2 nA dark current and an average responsivity over the visible spectrum $\eta = 0.3$. Moreover, with the aim of computing the receivers' noise, the analog front-end is modeled as a single amplifier stage (TIA) operated by a LTC6268-10 operational amplifier with 1 $pA/\sqrt{Hz}$ overall input-referred current noise. We further assumed that the N_r central-tier passengers were jointly served by $N_t \leq N_{t,tot}$ LEDs depending on the degree of coordination between emitting LEDs, while the remaining $N_I = N_{t,tot} - N_t$ LEDs contributed as uncoordinated interference that cannot be canceled by any mean, thus degrading the system performance. Following the avionic layout for lightings proposed in [31] and [32], we inserted 6 wash lights near the luggage compartment and pointed toward the ceiling, 2 ceiling lights in the center of the corridor ceiling and pointed downward and 6 side wall lights, as general LED illumination fixtures emitting a luminous intensity of 1980 lm (assuming a LED luminous efficacy of 90 lm/W) distributed on a neutral white spectrum of 5000 K and a beam angle of 70 degrees. Moreover, in order to consider the worst situation, we associated to each 3-seats group an airplane window of 25 $\times$ 25 cm size from which both the direct sunlight and the diffuse one (skylight) got

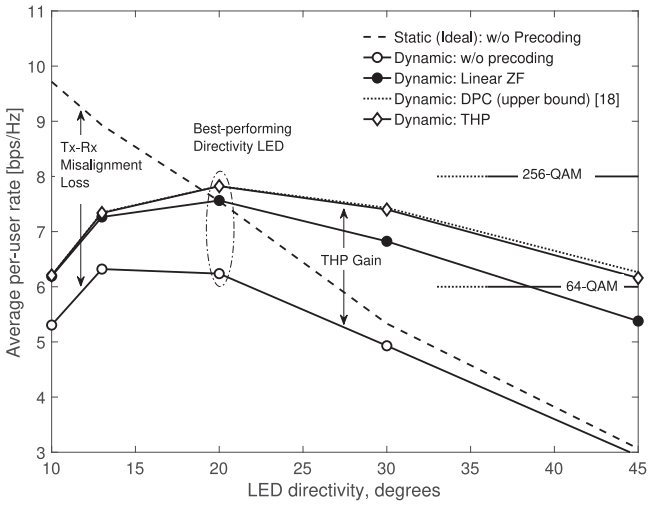

Fig. 4. Static (ideal) versus dynamic scenario: performance comparison by varying the LED directivity for different precoding schemes.

into. We computed the solar radiation in clear sky conditions (above clouds) at a reference altitude of 10000 m. Finally, the reading lamps were modeled by employing typical parameters for avionic applications [33] such as 100 lm average emitted luminous power, corresponding to $P_T = 0.58$ W, and the same 5000 K neutral white spectrum, while we let the lamp emission angle (i.e., directivity) varied in the simulations to find the optimal configuration for this specific application. In particular, we tested 5 beam angles Θ: 10, 13, 20, 30, 45 degrees, being the first two (10, 13) the most commonly deployed in today's airplane cabins [33] and the other three (20, 30, 45) chosen to investigate new possible solutions more suitable for the considered VLC on board Internet system where each passenger may reasonably move its the terminal deviating from the perfect alignment condition, but still maintaining the connectivity. The aim of our valuation was twofold: *i)* show the impact of Θ on the average amount of performance degradation (in terms of channel capacity) due to misalignment with respect to the ideal static case; *ii)* investigate the performance gain provided by precoding the transmitted signal when varying Θ and the degree of emitting LEDs coordination, i.e., the number of sources that are jointly precoding and transmitting signals to the same set of users. In this paper, we considered different degrees of transmitters coordination, so that the number of transmitting LEDs that perform joint precoding and transmission can be either 3 (the reading lamps belonging to the same 3-seats group), 6 (the lamps of the same seat-tier) or all the $N_{t,tot}$ lamps (i.e., fully coordinated system). In practice, since we assumed that each passenger can reasonably move its terminal around the perfect alignment condition, we generated for each passenger a set of 10 realistic movements chosen to efficiently sample the user's available space and assuming that the receiver displacement from the best light-beam alignment position along each of the three dimensions can range from 15 to 25 cm. Then, for each value of the beam angle Θ, we evaluated the performance by averaging the user-capacity (computed as in (26)) over 60 channel realizations. Precoder design under imperfect channel state information conditions is beyond the scope of the paper, hence, the precoding matrixes for ZFP in (27) and THP in (32) have been computed by assuming perfect channel knowledge at the transmitter side.

5.2 Results

The first set of results we present are plotted in Fig. 4. When the reading lamps are perfectly pointed toward the users' equipment (dashed line), the data-rate capacity of the links (computed with (22)) exhibits a monotonic decrease as the beam angle of the sources Θ increases: this effect is due to

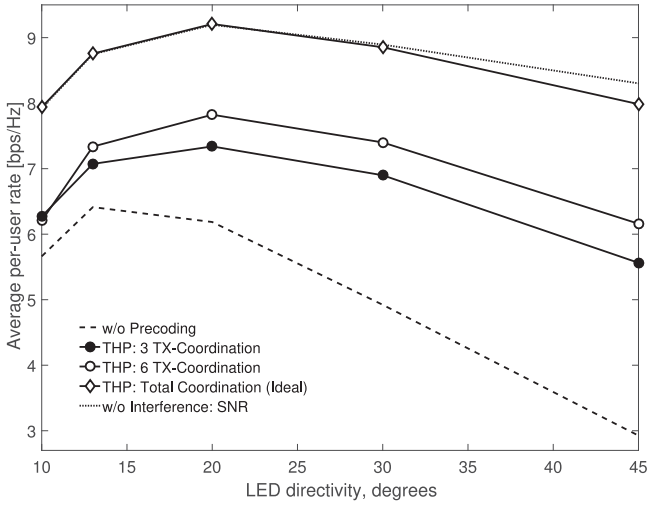

Fig. 5. Performance comparison varying the degree of transmitter coordination.

the increase of the MLI as well as to the decrease of the optical power density that impinges the receivers. When the receiving terminals move away (even slightly) from the center of the light cone of the lamps (solid lines), the performance degrades rapidly and the channel capacity, in case of precoding (considered here of degree 6), shows a peak for $\Theta_{\text{max}} = 20^{\circ}$. In fact, when $\Theta < \Theta_{\text{max}}$, the light cone of each LED is so narrow that when the users move, they can easily fall out of the coverage region, hence experiencing a drastic loss of signal power (inversely proportional to Θ) which limits the performance. By contrast, as $\Theta > \Theta_{\text{max}}$, the coverage area is enlarged and thus the misalignments' effect is less effective, but at the same time this implies a strong increment of MLI, from both coordinated and uncoordinated sources. As detailed in Sect. IV, TP completely cancels the MLI from the 6 coordinated sources, however, the performance of the system slightly decrease with Θ both for the residual, uncoordinated interference and for the loss of signal power (as for the static case). In this regard, $\Theta_{\text{max}} = 20^{\circ}$ turns out to be the best solution for dynamic scenarios, since it provides the best balancing between signal coverage (power) and residual MLI. As expected, the overall performance gain provided by TP increases proportionally to Θ (and thus to the amount of MLI): in particular, when employing THP, the achievable channel capacity for $\Theta = \Theta_{\text{max}} = 20^{\circ}$ is 7.88 bps/Hz, that can be considered high if compared to 5G point-to-point communications (whose associated maximum modulation format that can be employed is 256-QAM) [34]. The performance is upper-bounded by the theoretical limit provided by ZF-DPC (dotted line) [18], although THP almost matches such limit for most of the angles. Regarding the emission angle of the lamps, it is worth noting that, since their angular light distribution is optimized for providing a good passenger comfort (avoiding glare), the standard commercially available reading lamps for airplanes emit on a beam angle between 10° and 15°. When those lamps are also intended for communication, the average emitted power (and the consequent illumination level) is diminished to a certain extent with respect to the nominal one (e.g. halved as here): we can therefore think to relax the tight constraint on the angle, tolerating a wider one such as $\Theta = 20^{\circ}$, proved here to achieve the best performance even in case of transmitter-receiver misalignment.

The user-rate obtained for different levels of TX coordination when employing THP are depicted in Fig. 5, emphasizing the trade-off between achievable performance and system complexity of the implementation. As expected, the latter can be reduced, at the price of a performance loss, by decreasing the level of transmitters' cooperation from 6 (empty circle marker, used as reference in the previous result) to 3 (filled circle marker), which still provides remarkable benefits with respect to the unprecoded case (dashed line). Moreover, Fig. 5 shows that the utmost performance limit can be reached by fully centralizing the transmission (diamond marker): all the $N_{t,\text{tot}} = 18$ sources

in the cabin are coordinated to serve the $N_r = 6$ users. In this case all the MLI is suppressed by precoding, thus the performance match the SNR-limited ones. This condition is, however, unpractical in conventional aircraft VLC systems. Apart from the exponentially increasing precoder complexity of a fully centralized transmission, the coordination among sources of different tiers of seats is unfeasible: since the airplane fuselage in Fig. 3 is only a slice of the real one, precoding groups of 18 sources contemporarily leads to an undesirable unfairness in users' performance, inasmuch the passengers belonging to the frontal and rear seat tiers of each group (e.g., edge users) are affected by the interference of the adjacent, uncoordinated ones.

Remark 2: This work focuses on the Boeing 737 airplane cabin. However, some considerations on the possible effects of considering different scenarios can be made, since airplane cabins mainly differ from each other in the spatial arrangements of seats. Let us consider as an example the case of a two-corridor cabin (i.e., Boeing 777 [35]): in this case each seat-tier includes 10 seats divided into 3 groups of 3-4-3 (for Boeing 777-200) or 11 seats divided into 3-5-3 (for Boeing 777-300). The 4 (or 5) central passengers are mutually interfering as well as also interfered both by the passengers on the left and by those on the right. This challenging scenario is therefore characterized by stronger interference than the Boeing 737 considered in this paper, and that is the reason why the impact of the proposed non-linear precoding techniques will be even more evident.

6. Conclusion

In this paper, Tomlinson-Harashima Precoding (THP) scheme is proposed for on-board VLC systems in order to pre-compensate the strong MLI arising from the high number of adjacent transmitters (i.e., LED reading lamps), without any further complexity at receiver-side. THP guarantees a fair user performance even in the challenging case of transmitter-receiver misalignment due to the user terminals' movements. To assess the benefits of the proposed on-board VLC system, we performed numerical evaluations based on ray tracing-generated channels for a standard-equipped Boeing 737 fuselage. Numerical results confirm the effectiveness of the proposed THP based VLC system in providing high-speed connectivity to all the passengers: it not only outperforms conventional unprecoded VLC systems by more then 1.5 bps/Hz, but also linear Zero-Forcing precoded ones. Numerical simulations further showed that coordinating the 6 transmitters belonging to the same seat tier and employing 20° LED directivity presents the best trade-off between received power (high LED directivity), the amount of MUI (low LED directivity) and overall system complexity, thus providing robustness with respect to users' movements and still achieving almost 8 bps/Hz (256-QAM), used as ultimate target spectral efficiency for 5G communication systems.

References

[1] T. Komine and M. Nakagawa, "Fundamental analysis for visible-light communication system using LED lights," *IEEE Trans. Consum. Electron.*, vol. 50, no. 1, pp. 100–107, Feb. 2004. [Online]. Available: https://doi.org/10.1109/TCE.2004.1277847

[2] GoGo, "GoGo 2ku: High performance inflight connectivity," 2017. [Online]. Available: https://www.gogoair.com/assets/downloads/gogo-2ku-brochure.pdf

[3] V. Degardin, P. Laly, M. Lienard, and P. Degauque, "Investigation on power line communication in aircrafts," *IET Commun.*, vol. 8, no. 10, pp. 1868–1874, Jul. 2014.

[4] E. Chan, "Wireless optical links for airplane applications," in *Proc. IEEE Photon. Soc. Summer Top. Meeting*, Jul. 2012, pp. 76–77.

[5] D. Krichene, M. Sliti, W. Abdallah, and N. Boudriga, "An aeronautical visible light communication system to enable in-flight connectivity," in *Proc. 17th Int. Conf. Transparent Opt. Netw.*, Jul. 2015, pp. 1–6.

[6] I. H. Park, Y. H. Kim, and J. Y. Kim, "Interference mitigation scheme of visible light communication systems for aircraft wireless applications," in *Proc. IEEE Int. Conf. Consum. Electron.*, Jan. 2012, pp. 355–356.

[7] C. Quintana, V. Guerra, J. Rufo, J. Rabadan, and R. Perez-Jimenez, "Reading lamp-based visible light communication system for in-flight entertainment," *IEEE Trans. Consum. Electron.*, vol. 59, no. 1, pp. 31–37, Feb. 2013.

[8] D. Tagliaferri and C. Capsoni, "SNIR predictions for on-aircraft VLC systems," in *Proc. Int. Conf. Broadband Commun. Next Gener. Netw. Multimedia Appl.*, Sep. 2016, pp. 1–7.

[9] P. H. Pathak, X. Feng, P. Hu, and P. Mohapatra, "Visible light communication, networking, and sensing: a survey, potential and challenges," *IEEE Commun. Surv. Tut.*, vol. 17, no. 4, pp. 2047–2077, Fourth Quarter 2015.

[10] J. M. Luna-Rivera, R. Perez-Jimenez, J. A. Rabadan-Borjes, J. F. Rufo-Torres, V. Guerra, and C. Suarez-Rodriguez, "Multiuser scheme for indoor visible light communications using RGB leds," in *Proc. 3rd IEEE Int. Work-Conf. Bioinspired Intell.*, Jul. 2014, pp. 119–123.
[11] K. Zhou, C. Gong, Q. Gao, and Z. Xu, "Inter-cell interference coordination for multi-color visible light communication networks," in *Proc. IEEE Global Conf. Signal Inf. Process*, Dec. 2016, pp. 6–10.
[12] R. F. Fischer, C. Windpassinger, A. Lampe, and J. B. Huber, "Space-time transmission using tomlinson-harashima precoding," in *Proc. ITG FACHBERICHT*, 2002, pp. 139–148.
[13] M. Joham, J. Brehmer, and W. Utschick, "MMSE approaches to multiuser spatio-temporal tomlinson-harashima precoding," in *Proc. ITG FACHBERICHT*, 2004, pp. 387–394.
[14] T. Fath and H. Haas, "Performance comparison of MIMO techniques for optical wireless communications in indoor environments," *IEEE Trans. Commun.*, vol. 61, no. 2, pp. 733–742, Feb. 2013.
[15] C. W. Hsu, C. W. Chow, I. C. Lu, Y. L. Liu, C. H. Yeh, and Y. Liu, "High speed imaging 3 $\times$ 3 MIMO phosphor white-light led based visible light communication system," *IEEE Photon. J.*, vol. 8, no. 6, Dec. 2016, Art. no. 7907406.
[16] B. Li, J. Wang, R. Zhang, H. Shen, C. Zhao, and L. Hanzo, "Multiuser miso transceiver design for indoor downlink visible light communication under per-led optical power constraints," *IEEE Photon. J.*, vol. 7, no. 4, Aug. 2015, Art. no. 7201415.
[17] H. Ma, L. Lampe, and S. Hranilovic, "Coordinated broadcasting for multiuser indoor visible light communication systems," *IEEE Trans. Commun.*, vol. 63, no. 9, pp. 3313–3324, Sep. 2015.
[18] Z. Yu, R. J. Baxley, and G. T. Zhou, "Multi-user MISO broadcasting for indoor visible light communication," in *Proc. IEEE Int. Conf. Acoust., Speech Signal Process.*, May 2013, pp. 4849–4853.
[19] T. V. Pham, H. Le-Minh, and A. T. Pham, "Multi-user visible light communication broadcast channels with zero-forcing precoding," *IEEE Trans. Commun.*, vol. 65, no. 6, pp. 2509–2521, Jun. 2017.
[20] C. A. Gueymard, "Parameterized transmittance model for direct beam and circumsolar spectral irradiance," *Solar Energy*, vol. 71, no. 5, pp. 325–346, 2001. [Online]. Available: http://www.sciencedirect.com/science/article/pii/S0038092X01000548
[21] R. E. Bird and C. J. Riordan, "Simple simple solar spectral model for direct and diffuse irradiance on horizontal and tilted planes at the earth's surface for cloudless atmospheres," *J. Climate Appl. Meteorol.*, vol. 25, no. 1, pp. 87–97, Jan. 1986.
[22] S. P. Rodríguez, R. P. Jiménez, B. R. Mendoza, F. J. L. Hernández, and A. J. A. Alfonso, "Simulation of impulse response for indoor visible light communications using 3d cad models," *EURASIP J. Wireless Commun. Netw.*, vol. 2013, no. 1, pp. 1–10, Jan. 2013. [Online]. Available: https://doi.org/10.1186/1687-1499-2013-7
[23] J. M. Kahn and J. R. Barry, "Wireless infrared communications," *Proc. IEEE*, vol. 85, no. 2, pp. 265–298, Feb. 1997.
[24] A. Lapidoth, S. M. Moser, and M. A. Wigger, "On the capacity of free-space optical intensity channels," *IEEE Trans. Inf. Theory*, vol. 55, no. 10, pp. 4449–4461, Oct. 2009.
[25] Cree. "cree PLCC2 1 in 1 SMD LED CLM1C-WKW," 2017. [Online]. Available: http://www.cree.com/led-components/media/documents/CLM1CWKW(879).pdf
[26] Q. Wang, Z. Wang, and L. Dai, "Multiuser MIMO-OFDM for visible light communications," *IEEE Photon. J.*, vol. 7, no. 6, Dec. 2015, Art. no. 7904911.
[27] Q. H. Spencer, A. L. Swindlehurst, and M. Haardt, "Zero-forcing methods for downlink spatial multiplexing in multiuser mimo channels," *IEEE Trans. Signal Process.*, vol. 52, no. 2, pp. 461–471, Feb. 2004.
[28] G. Ginis and J. M. Cioffi, "Vectored transmission for digital subscriber line systems," *IEEE J. Sel. Areas Commun.*, vol. 20, no. 5, pp. 1085–1104, Jun. 2002.
[29] M. Hekrdla, A. Matera, W. Wang, D. Wei, and U. Spagnolini, "Ordered tomlinson-harashima precoding in g. fast downstream," in *Proc. IEEE Global Commun. Conf.*, 2015, pp. 1–6.
[30] Boeing. "737 airplane characteristics for airport planning," 2013. [Online]. Available: http://www.boeing.com/assets/pdf/commercial/airports/acaps/737.pdf
[31] U. T. C. Aerospace. "LED wash lights 1005-x1x-001," 2016. [Online]. Available: https://www.utcaerospacesystems.com/
[32] U. T. C. Aerospace. "LED wash lights retrofit 2la45665y-xx," 2017. [Online]. Available: https://www.utcaerospacesystems.com/
[33] U. T. C. Aerospace. "LED reading lights," 2015. [Online]. Available: https://www.utcaerospacesystems.com/
[34] 3rd G. P. P., *3GPP TS 38.211 V15.0.0 (2017-12)*, 2017. [Online]. Available: http://www.3gpp.org/ftp//Specs/archive/. Accessed on: Jan. 15, 2018.
[35] Boeing. "777-200/300 airplane characteristics for airport planning," 2013. [Online]. Available: http://www.boeing.com/assets/pdf/commercial/airports/acaps/777-23.pdf